



Dual-Polarized Phased Array with Endfire Radiation for 5G Handset Applications

Zhang, Jin; Zhao, Kun; Wang, Lei; Zhang, Shuai; Pedersen, Gert Frølund

Published in:
I E E E Transactions on Antennas and Propagation

DOI (link to publication from Publisher):
[10.1109/TAP.2019.2937584](https://doi.org/10.1109/TAP.2019.2937584)

Creative Commons License
Unspecified

Publication date:
2020

Document Version
Accepted author manuscript, peer reviewed version

[Link to publication from Aalborg University](#)

Citation for published version (APA):
Zhang, J., Zhao, K., Wang, L., Zhang, S., & Pedersen, G. F. (2020). Dual-Polarized Phased Array with Endfire Radiation for 5G Handset Applications. *I E E E Transactions on Antennas and Propagation*, 68(4), 3277-3282. [8822604]. <https://doi.org/10.1109/TAP.2019.2937584>

General rights

Copyright and moral rights for the publications made accessible in the public portal are retained by the authors and/or other copyright owners and it is a condition of accessing publications that users recognise and abide by the legal requirements associated with these rights.

- Users may download and print one copy of any publication from the public portal for the purpose of private study or research.
- You may not further distribute the material or use it for any profit-making activity or commercial gain
- You may freely distribute the URL identifying the publication in the public portal -

Take down policy

If you believe that this document breaches copyright please contact us at vbn@aub.aau.dk providing details, and we will remove access to the work immediately and investigate your claim.

Communication

Dual-Polarized Phased Array with Endfire Radiation for 5G Handset Applications

Jin Zhang, Kun Zhao, Lei Wang, *Member, IEEE*, Shuai Zhang, *Senior Member, IEEE*,
and Gert Frølund Pedersen, *Senior Member, IEEE*

Abstract—This paper proposes a dual-polarized endfire phased array for 5G handset devices at 28 GHz. The proposed 4-element array has low profile of 1.1 mm, small clearance of 2.7 mm, and symmetric patterns in the vertical plane. The array element is fed by Substrate Integrated Waveguide (SIW), which works as a waveguide (WG) antenna with vertically polarized radiation pattern. Two transition plates are introduced to improve the impedance matching of the WG antenna. The horizontal polarization is generated by exciting one of the transition plate as an antenna. The other transition plate is modified as a group of triangle strips to minimize its reflection to the horizontal radiation patterns. A -10-dB frequency bandwidth of 5.3% and a -6-dB bandwidth of 25% are achieved, overlapping between the vertical and horizontal polarization. The array scanning angle is from -54° to 44° at 29 GHz for both polarization. Within the scanning range, the endfire gain varies from 7.48 to 8.14 dBi for the horizontal polarization, whereas from 4.49 to 8.05 dBi for the vertical polarization. Good agreements between simulations and measurements are well achieved and shown in this paper.

Index Terms—5G communication, antennas for handset devices, dual-polarization, phased array, SIW.

I. INTRODUCTION

The achievement of high data rate is one of the key features in the 5G communication systems. At millimeter wave (mm-wave) band a large spectrum is available and therefore, it is a good candidate to be used for cellular mobile systems. Because of the high path loss at these frequencies, phased arrays with high gain have to be adopted [1], [2]. An advantage of the dual-polarized antenna arrays over the single-polarized is the fact that they may provide better connection with the base stations due to the unpredictable orientation of the handset devices. Over the past years, significant progress has been made on the dual-polarized antennas for base station applications of the 2G/3G/LTE communication systems. In [3], [4], they have been introduced a dual-polarized patch antenna with differential feedings. Large bandwidth is achieved by exciting two orthogonal dipole, as shown in [5]–[10]. Those antennas have the advantages of wideband, low cross-polarization, and symmetric radiation patterns. However, the 3D structures of the antenna and feeding networks are difficult to realized in mm-wave band due to the shrinking of antenna size.

A dual-polarized planar aperture antenna at 60 GHz is presented in [11]. Low-temperature cofired ceramics (LTCC) technology is adopted to realize the multi-layer stacked structure. Another dual-polarized antenna at 60 GHz is shown in [12]. A magneto-electric

This work was supported by the AAU Young Talent Program and in part by the Innovations Fonden Project of RANGE (Corresponding author: Shuai Zhang).

J. Zhang, S. Zhang (e-mail: sz@es.aau.dk) and G. F. Pedersen are with the Antennas, Propagation and Millimeter-wave Systems, Department of Electronic Systems, Aalborg University, 9220 Aalborg Ø, Denmark.

K. Zhao is with research and standardization, Sony Mobile Communications AB, 22188 Lund, Sweden and is also with the Antennas, Propagation and Millimeter-wave Systems, Department of Electronic Systems, Aalborg University, 9220 Aalborg Ø, Denmark.

L. Wang is with the Institute of Electromagnetic Theory, Hamburg University of Technology, 21079 Hamburg, Germany (e-mail: wanglei@ieee.org).

dipole is excited by two stacked slots and it has been used in a 2×2 array as an array element. They are designed for 60 GHz but the current frequency bands of 5G system will be mainly deployed around 28 GHz [13]. If the same strategy is applied at 28 GHz, the volume of the antenna will be much thicker than at 60 GHz. Moreover, all these antennas have broadside radiation patterns. However, the endfire arrays are more preferred in the mobile handsets [14], [15]. The antennas in [16], [17] realized endfire dual-polarized radiation patterns by applying multi-layer PCB. In [18] has been presented horizontal and vertical polarized Yagi-Uda antennas integrated together in order to achieve both linear polarization with endfire radiation patterns. Due to the fact that the thickness of the substrate has to be quarter wavelength at the operating frequency, it is quite difficult to lower the antenna profile. Moreover, because of the asymmetric structure in [16], [18], the radiation patterns are also tilted in the elevation plane. A dual-polarization SIW WG antenna is proposed in [19] with low profile but it is not easy to be integrated into a handset device due to the big electrical size.

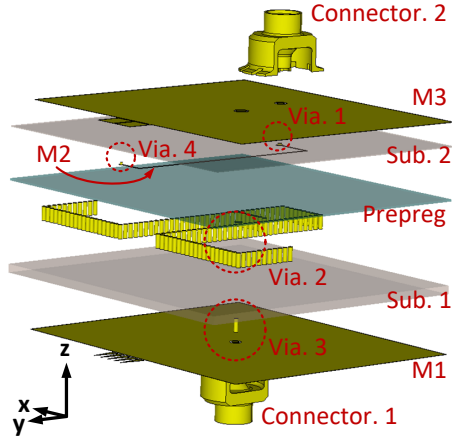
In this paper, a dual-polarized endfire phased array, which has low profile, small clearance, and symmetric patterns in the vertical plane, is proposed for 5G handset applications at 28 GHz. The paper is organized as follows. Section II introduces the antenna design and analyze it. In Section III the simulated and measured results of the antenna array are presented. Finally, conclusion is provided in Section VI.

To avoid potential confusion, the $\pm y$ direction in the following content is called endfire direction, which is defined according to the mobile phone or the ground plane. To simplify the description, the vertical polarization (V-pol) and the horizontal polarization (H-pol) are used to represent the θ polarization and the ϕ polarization in this paper, respectively.

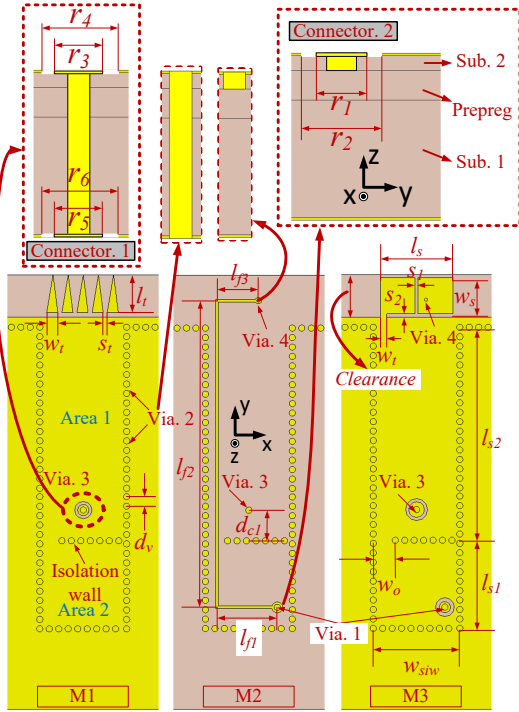
II. ANTENNA DESIGN AND ANALYSIS

A. Array Element Structure

The array element configuration is shown in Fig.1. The antenna is constructed by a two-layer stack-up PCB: Sub. 1, Sub. 2, and a prepreg layer between them, as shown in Fig.1a. The material of Sub. 1 is Rogers RO4003C ($\epsilon_r = 3.38$, $\tan\delta = 0.0025$), Sub. 2 is Rogers RO4350B ($\epsilon_r = 3.66$, $\tan\delta = 0.0037$), and prepreg is Rogers RO4450F ($\epsilon_r = 3.7$, $\tan\delta = 0.004$). The thickness of Sub. 1 is 0.8 mm, Sub. 2 is 0.1 mm, and prepreg is 0.2 mm. The thickness of the metallic layers (M1, M2, and M3 in Fig.1a) is $18 \mu\text{m}$ each. Connector. 1 and Connector. 2 are the feeding ports for the V and H modes, respectively. Connector. 1 is mounted on M1 and connector. 2 is mounted on M3. The two connectors can also be put on the same side of the PCB. In this case, the radiation patterns in the vertical plane will be slightly tilted due to the asymmetric construction. If it is necessary to have both connectors on one side, the transition plates should also be modified to compensate the influence of the connectors. The structures on M1, M2, and M3 are shown in Fig.1b.

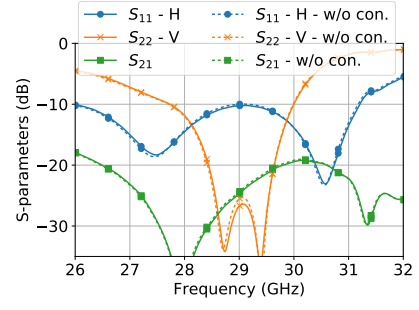


(a)

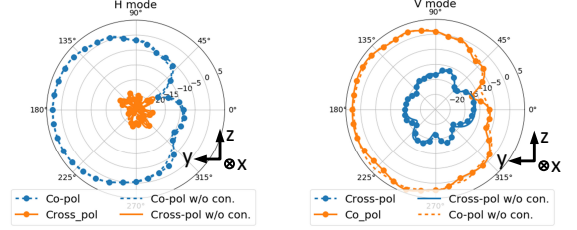


(b)

Fig. 1: Antenna configuration. (a) Exploded view. (b) Dimensions on layers.

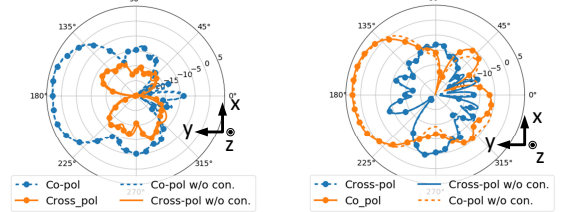


(a)



(b)

(c)



(d)

(e)

Fig. 2: The simulation results of the proposed antenna with and without connectors at 29 GHz. (a) The S-parameters. (b) The radiation patterns of the H mode in the vertical plane (yoz). (c) The radiation patterns of the V mode in the vertical plane (yoz). (d) The radiation patterns of the H mode in the horizontal plane (xoy). (e) The radiation patterns of the V mode in the horizontal plane (xoy).

TABLE I: The Dimensions of the Proposed Antenna. (Units: mm)

w_t	s_t	l_t	r_1	r_2	r_3	r_4	r_5	r_6
0.7	0.26	2.4	0.35	0.6	0.5	0.7	0.35	0.55
w_{siw}	l_{s1}	l_{s2}	w_o	w_s	l_s	s_1	s_2	l_{f1}
5.5	5.6	13.6	1.4	2.3	4.6	0.2	0.2	3.83
l_{f2}	l_{f3}	d_{c1}	d_v	w_t	ϕ_1	ϕ_2	ϕ_3	ϕ_4
19	2.6	2.25	0.6	0.4	0.4	0.4	0.4	0.2

The depth of each via is shown in the cross section view in the zoom-in pictures in Fig.1b. The diameter of each via is ϕ_i , $i = 1, 2, 3, 4$. Via. 2 are a set of metallic vias, which form the sidewall of SIW. The array element is designed on a $30 \text{ mm} \times 27.7 \text{ mm}$ ground plane. The clearance is defined as the clean area reserved on the ground plane for the antennas, which in this paper is from the top of the substrate until the edge of the copper. The clearance is 2.7 mm on both M1 and M3, as shown in Fig.1b. All the other dimensions are listed in Table.I.

B. Analysis of H mode (ϕ Polarization)

The transition plates are adopted to improve the impedance matching of the SIW WG antenna (V-pol) [20]. In the proposed antenna,

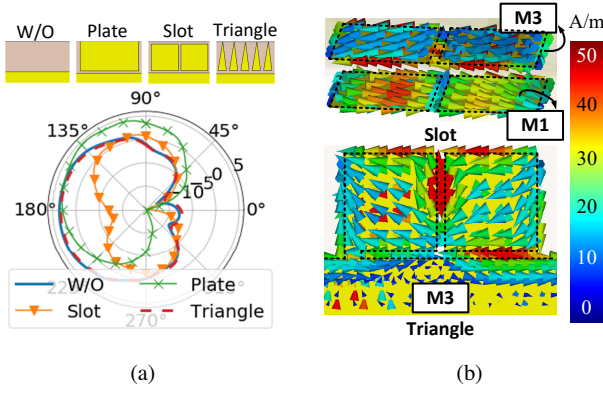


Fig. 3: The influence of different plates on M1 to the H-pol radiation patterns at 28 GHz. (a) The radiation patterns in the vertical plane (yoz). (b) The surface current distribution.

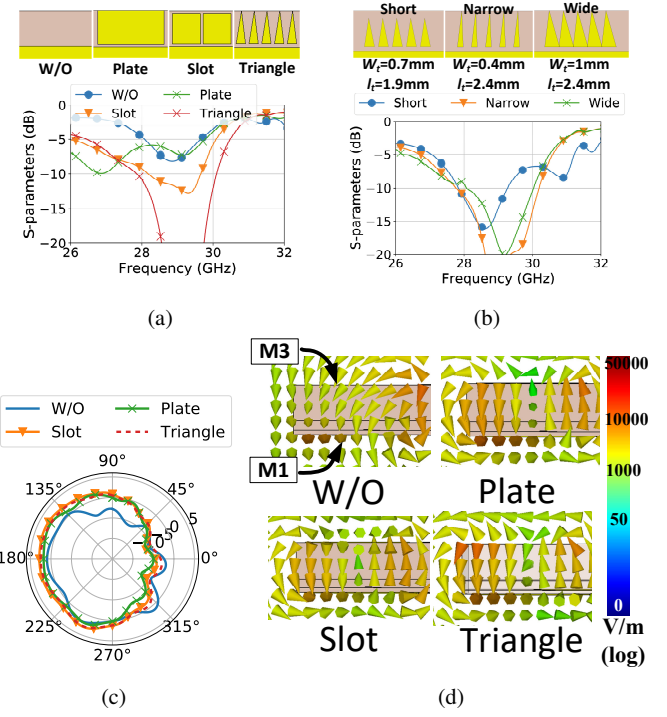


Fig. 4: The reflection coefficients and radiation patterns of the V mode with different plates on M1. (a) Reflection coefficients with different plates. (b) Reflection coefficients with different dimensions of the triangle strips. (c) Radiation patterns in the vertical plane (yoz). (d) The V mode E-field distribution at 28 GHz with different transition plates on M1 (yoz).

the transition plate on M3 is modified in order to generate H-pol radiation. As shown in Fig.1b, the transition plate on M3 is modified as two patches and stimulated by a strip line on M2. The patch on the left is connected with the ground plane for supporting the microwave propagation on the strip line. The strip line is fed by Connector. 2 through Via. 1 and connects with the patch on the right through Via. 4. The energy from the strip line is coupled to the patches through the slot between them. The two patches can be considered as two arms of a dipole antenna, which generates an H-pol endfire radiation pattern. An isolation wall divides the SIW cavity into Area 1 and Area 2. An opening on the left side of the isolation wall is made to let the strip line pass. In this way, it is easier to reach good impedance matching of the V mode. The isolation between the two ports is also improved because the TE₁₀ mode is limited in Area 1.

The other transition plate is on M1 and consists of some triangle metal strips. The tapered transition plates are introduced to further improve the radiation and the impedance matching [21]. They are usually the same on both sides of PCB to provide a symmetric boundary for the SIW aperture and further guarantee the radiation pattern to be symmetric in the vertical plane. However, the same condition is hard to satisfy in this dual-polarization design. Fig.3a shows the radiation patterns in the vertical plane (yoz) of H mode at 28 GHz with different plates on M1. When no plate is on M1, it has the endfire radiation pattern. When a whole plate is on M1, the main beam is reflected by the plate and tilted to the +z direction. If the plate on M1 is identical as M3 (Slot), a null is observed in the endfire direction. It turns out that the triangle strips have little influence to the H-pol radiation pattern, which keeps the same shape as the one without plate. It can be explained by the "Slot" surface current distribution in Fig.3b. The currents on M1 have the same magnitude and opposite direction with the radiating plates on M3. So the radiation from the plates on both sides cancels out in the endfire direction. The currents on a whole plate are weaker than "Slot" so the radiation pattern is closer to endfire. As the triangle strips are adopted, the current magnitude is much reduced and the direction is also changed. As a result, the radiation pattern still keeps endfire.

The surface current distribution on M3 of H mode is shown in Fig.3b as "Triangle". A reverse "T" shape slot is formed by the patches and the ground plane. The radiation of the slot can be divided into two parts: part from the slot in the middle of the transition plate (Slot 1) and part from the slot between the transition plate and the ground plane (Slot 2). The magnetic current on Slot 1 generates the H-pol and endfire radiation pattern, while Slot 2 radiates to the +/-z directions and θ polarized pattern. On the other hand, the current

on the two patches has the same direction, which also has an H-pol endfire radiation pattern. Therefore, the co-pol part of the H mode consists of the radiation from the electric current on the transition plates and the magnetic current from Slot 1. The radiation of Slot 2 contributes to the cross-pol part.

C. Analysis of V mode (θ Polarization)

The reflection coefficients and radiation patterns at 28 GHz of the V mode in the vertical plane are shown in Fig.4a with different plates on M1. The impedance matching and bandwidth is different when the shape of the plates changes due to different coupling of the aperture and the plates. The scenario without plate (W/O) has the worst matching and the narrowest bandwidth while the patterns of the plate improves the bandwidth. When there is no plate on M1, the radiation patterns in Fig.4c tilt to the -z direction. When the plate exists, the radiation patterns are similar to the endfire and symmetric shape. The impedance matching of the V mode can be controlled by the shape of the triangle strips, as shown in Fig.4b. The main beam direction of the V mode can be slightly adjusted by changing the length of the triangle strips but it will cause the changing of impedance matching as well.

The E-field distribution with different transition plates at 28 GHz is shown in Fig.4d. As we can see, with both plates on M1 and M3, the E-field on the antenna aperture has vertical polarization and the magnitude distributes evenly. If there is no plate on M1, the polarization on the aperture changes and the E-field is stronger on the M3 layer. Therefore, the transition plates on both M1 and M3 are important for supporting the V-pol field.

In summary, the V mode requires a plate on M1 to improve the impedance matching but the radiation pattern is not sensitive to

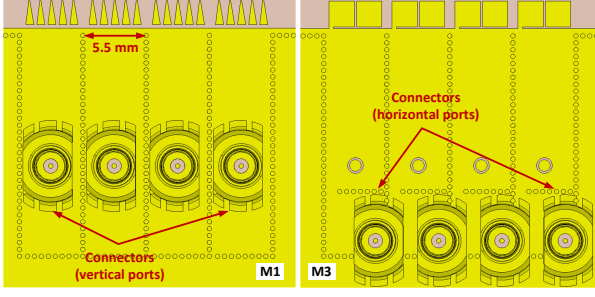


Fig. 5: The array configuration in the simulation.

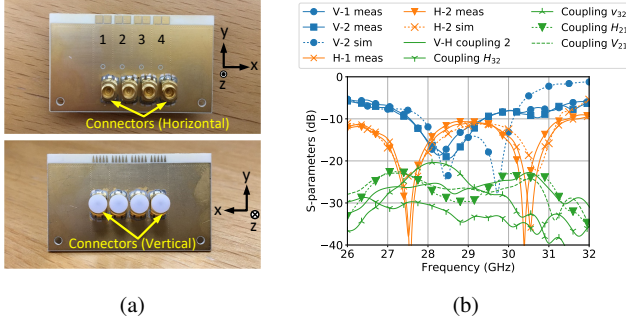


Fig. 6: The fabricated array model and the S-parameters. (a) The fabricated array model. (b) The simulated and measured S-parameters.

the shape of the plate. The triangle strips are chosen because of maintaining the endfire radiation of H mode as previously discussed.

III. SIMULATED AND EXPERIMENTAL RESULTS

Due to the high path loss of mm-wave, antenna array is needed for the user equipment (UE). The 4-element arrays are a promising solution [22]. The configuration of the proposed 4-element array is shown in Fig.5. The element distance is 5.5 mm, which is close to half wavelength of 28 GHz. The fabricated antenna model is shown in Fig.6a. Fig.6b shows the measured S-parameters of all the array elements and the simulated results of element 2 as comparisons. "V-1" and "V-2" represent the reflection coefficients of the V-pol ports of array element 1 and array element 2. "H-1" and "H-2" represent the reflection coefficients of the H-pol ports of the same array elements. The simulated and measured reflection coefficients of H mode show good impedance matching in a wide band, while the V mode has narrower bandwidth. The V mode has two resonances in the simulation but only one is observed in the measurement. It is because the resonance of V mode has higher Q value, which is more sensitive to the fabrication accuracy. The measured overlapped 10-dB bandwidth is 5.3% from 27.5 GHz to 29 GHz and the 6-dB bandwidth is 25% from 26.6 GHz to 34.3 GHz. Three curves are shown to present the measured mutual couplings. "V-H coupling 2" is the coupling between the V-pol and the H-pol ports of array element 2. "Coupling H_{ij} " is the coupling between the two H-pol ports from array element i and j . "Coupling V_{ij} " is the coupling between the two V mode ports from array element i and j . The other couplings are measured but not shown in this figure for simplicity. All of them are below -20 dB in the measurements.

The radiation patterns are measured in the anechoic chamber. The setup is shown in Fig.7. The under-test antenna is installed on a rotational axis. The area behind the array within 90° is blocked by the absorber so the radiation in that area cannot be measured. The

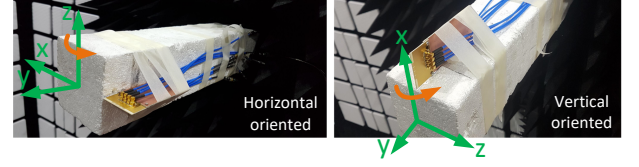


Fig. 7: The setup in the radiation pattern measurements.

array is measured in both vertically and horizontally oriented cases. The radiation patterns are simulated and measured from 27.5 GHz to 30 GHz. All the array elements have similar performances, to simplify the figures, only the results of element 2 are demonstrated. The radiation patterns in the vertical plane (yoz) of the two polarization modes are shown in Fig.8. Fig.8a, Fig.8c, Fig.8e, and Fig.8g are the radiation patterns of H mode, whereas Fig.8b, Fig.8d, Fig.8f, and Fig.8h are radiation patterns of V mode. The radiation patterns in the horizontal plane (xoy) are shown in Fig.9. Fig.9a, Fig.9c, Fig.9e, and Fig.9g are the radiation patterns of H mode and Fig.9b, Fig.9d, Fig.9f, and Fig.9h are the radiation patterns of the V mode. The measure co-polarized gain of the H mode at the 27.5GHz, 28 GHz, 29 GHz, and 30 GHz are 5.2 dBi, 5.07 dBi, 3.88 dBi, and 4.48 dBi, respectively. The measure co-polarized gain of the V mode at the 27.5GHz, 28 GHz, and 29 GHz are 4.77 dBi, 6.68 dBi, 6.75 dBi, and 4.3 dBi, respectively. The measured radiation patterns are symmetric in the vertical plane and most of them match very well with the simulations. The cross-pol level is 10 dB lower than the co-pol for both polarization. In addition, the cross-pol of the V mode is higher comparing with H mode because some currents on the ground plane leak to the squared transition plates through the connection and then participate in the radiation. Unfortunately, this connection is important for supporting the feeding of H mode and cannot be removed.

The simulated beam scanning patterns at 29 GHz are shown in Fig.10. Both the H and V mode cover from -54° to 44° , where the realized gain is above 0 dBi (-42° to 39° above 4 dBi). The beam scanning range is defined according to a certain gain level in order to measure the coverage of the scanning patterns at the same gain. The peak gain ranges from 7.48 dBi to 8.14 dBi for the H mode and from 4.49 dBi to 8.05 dBi for the V mode. The V and H modes have similar gain from 0° to 44° . The H mode has higher gain than the V mode from -54° to 0° . Because the array elements have wider and more symmetric beams in the H mode, as shown in Fig.9.

The materials of the mobile phone has influence to the mm-wave antenna performances [15]. The proposed array is simulated in a simplified mobile phone model in order to observe the performances in an actually-supposed handset, while only the results of array element 2 are presented, as shown in Fig.11a. It contains a plastic frame ($\epsilon_r = 3$), a glass front and back cover ($\epsilon_r = 6.84$, $\tan\delta = 0.0297$), a screen ($\epsilon_r = 4.82$, $\tan\delta = 0.0054$), and a phone PCB containing components which are modeled by copper. The size of the plastic frame is $142.9 \text{ mm} \times 73.9 \text{ mm}$. It covers the edges, the full back side, and 5.85 mm on the top of the front side. The glass covers on the front and back are 5.85 mm shorter than the plastic frame. The proposed array is placed on the top corner, which is covered by the plastic frame but not the glass covers and the screen. The square holes, which are opened on the covers, frame, and screen, are for the connectors in the simulations. The impedance matching and radiation patterns will change due to the different boundary conditions in the phone model comparing with free space. Some parameters are slightly tuned in the simulations with mobile phone model in order to reach good impedance matching ($l_t = 2.2 \text{ mm}$,

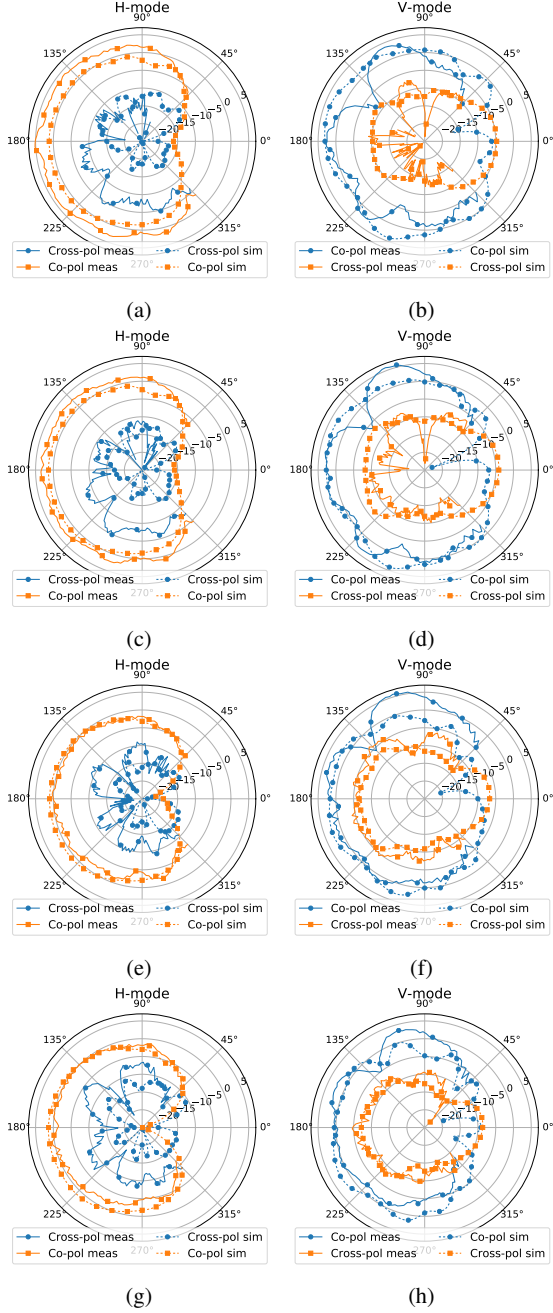


Fig. 8: The simulated and measured radiation patterns of array element 2 in the vertical plane (yoz). (a) H-mode at 27.5 GHz. (b) V-mode at 27.5 GHz. (c) H-mode at 28 GHz. (d) V-mode at 28 GHz. (e) H-mode at 29 GHz. (f) V-mode at 29 GHz. (g) H-mode at 30 GHz. (h) V-mode at 30 GHz.

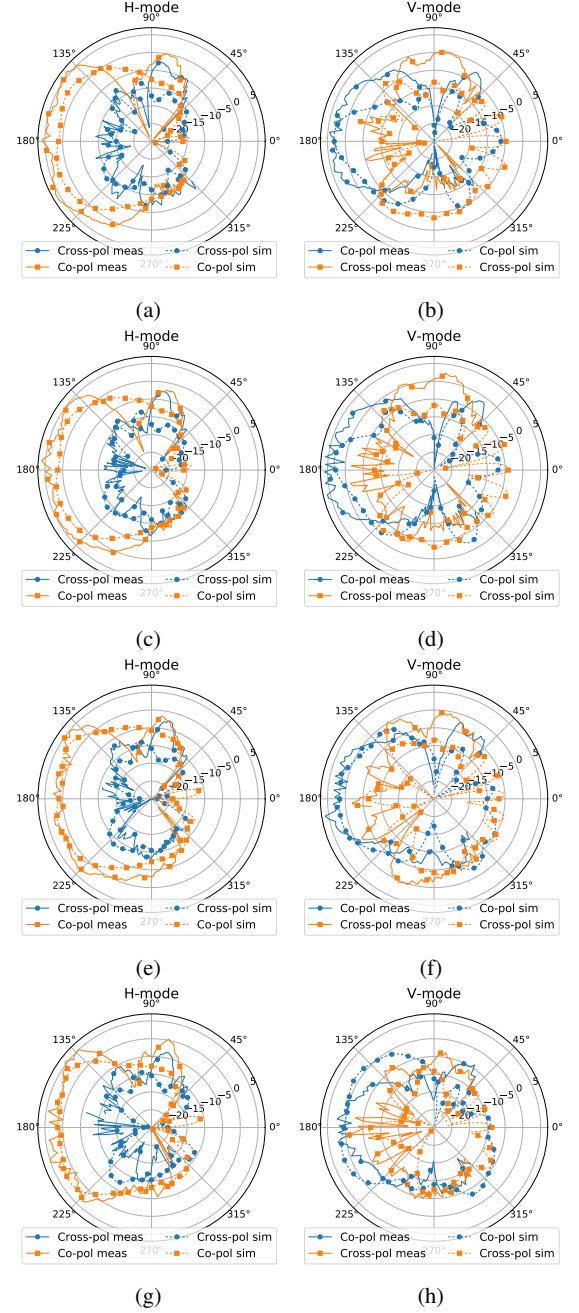


Fig. 9: The simulated and measured radiation patterns of array element 2 in the horizontal plane (xoy). (a) H-mode at 27.5 GHz. (b) V-mode at 27.5 GHz. (c) H-mode at 28 GHz. (d) V-mode at 28 GHz. (e) H-mode at 29 GHz. (f) V-mode at 29 GHz. (g) H-mode at 30 GHz. (h) V-mode at 30 GHz.

275 $s_2 = 0.1 \text{ mm}$, $d_{c1} = 2.05 \text{ mm}$). In Fig.11b, " $S_{H,H}$ ", " $S_{V,V}$ ", and
 276 " $S_{V,H}$ " represents the H-pol and V-pol reflection coefficients and
 277 coupling of the array element 2 without the phone model. " $S_{H,H}$
 278 phone", " $S_{V,V}$ phone", and " $S_{V,H}$ phone" are the results of the same
 279 array element with the phone model. The radiation patterns of array
 280 element 2 are presented at 28 GHz. Fig.11c and Fig.11d are the
 281 patterns of H mode in the vertical (yoz) and horizontal plane (xoy).
 282 Fig.11e and Fig.11f are the V mode in vertical (yoz) and horizontal
 283 plane (xoy). "co-pol phone" and "cross-pol phone" represent the co-
 284 pol and cross-pol patterns with the phone model, respectively. The

bandwidth of the V mode in the phone model is wider than that
 in free space but the radiation efficiency is nearly the same. As the
 comparison, both modes with phone model operate similarly as those
 in free space, which proves that the proposed array is compatible with
 a real mobile phone environment.

In Table.II, the performance of the proposed antenna is compared
 with some other mm-wave antennas, which has the potential to be
 implemented in handsets. The operating band is chosen according
 to the overlapping -10 dB impedance matching band of the two
 polarizations. The work in [11], [12], [16], [17], and [18] are dual

TABLE II: Comparison with Other Dual-Polarized Mm-wave Antennas Potential for Implementing in Handsets.

Ref No.	Antenna Type	Polarization	Beam Symmetry	Beam Direction	Array	Operating Band (GHz)	Element (dB)	Gain	Thickness	Clearance
[11]	Patch	Dual	N.A.	Broadside	No array	57 - 64	11 dBi		$0.226\lambda_0$	12 mm ($2.4\lambda_0$)
[12]	EM Dipole	Dual	N.A.	Broadside	2×2	53 - 71	8.4 dBi		$0.3\lambda_0$	5 mm ($1\lambda_0$)
[16]	Meshed patch	Dual	No	Endfire	1×16	56 - 68	3.8/4.5 dBi		$0.12\lambda_0$	0.75 mm ($0.15\lambda_0$)
[17]	SIW horn	Dual	Yes	Endfire	1×8	50 - 70	6.8 dBi		$0.66\lambda_0$	2.86 mm ($0.572\lambda_0$)
[18]	Yagi	Dual	No	Endfire	1×4	34 - 38	7 dBi		$0.23\lambda_0$	12.8 mm ($1.54\lambda_0$)
[23]	SIW Patch	Vertical	Yes	Endfire	1×4	29.45 - 33.4	6.6 dBi		$1\lambda_0$	0.508 mm ($0.05\lambda_0$)
[24]	Dipole	Vertical	Yes	Endfire	1×4	27 - 29	7.13 dBi		$0.46\lambda_0$	7 mm ($0.65\lambda_0$)
This work	SIW horn	Dual	Yes	Endfire	1×4	27.5 - 29.5	5 dBi		$0.1\lambda_0$	2.7 mm ($0.25\lambda_0$)

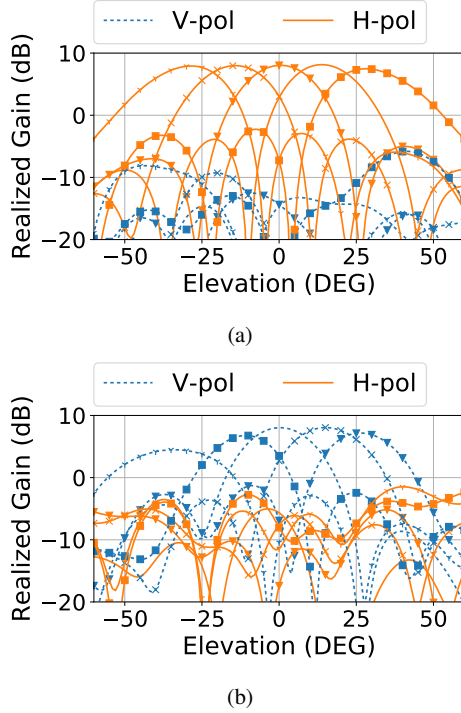


Fig. 10: The simulated scanning patterns in the horizontal plane (xoy). (a) H-mode at 29 GHz. (b) V-mode at 29 GHz.

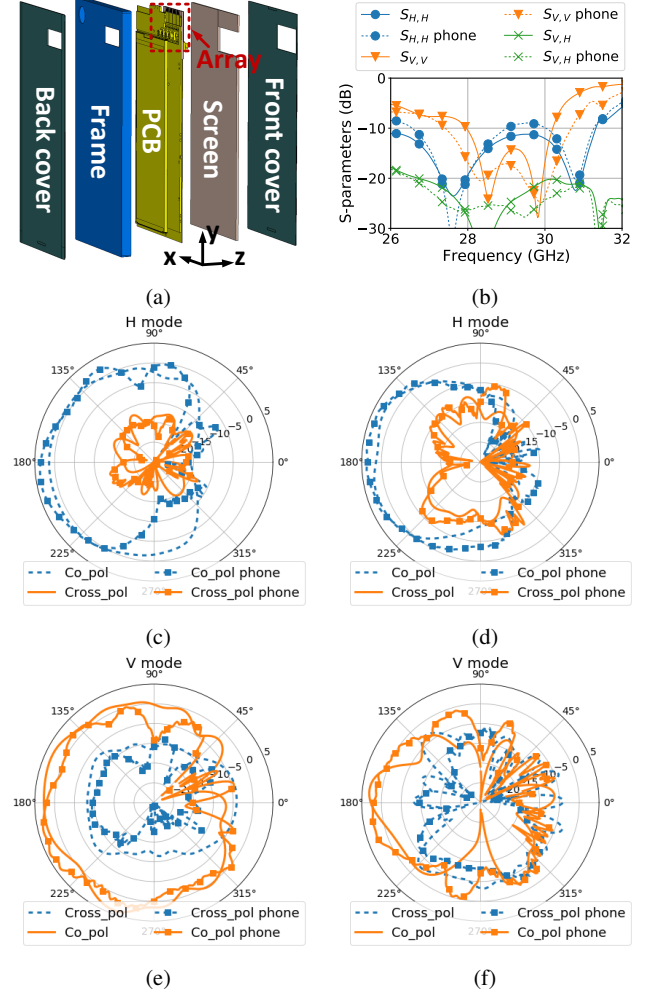


Fig. 11: The simulations of the proposed array in a mobile phone model at 28 GHz. (a) The array in the phone. (b) S-parameters of element 2 in the phone. (c) Radiation pattern of H-pol in the vertical plane (yoz). (d) Radiation pattern of H-pol in the horizontal plane (xoy). (e) Radiation pattern of V-pol in the vertical plane (yoz). (f) Radiation pattern of V-pol in the horizontal plane (xoy).

linearly polarized antennas. The work in [23] and [24] are two vertically polarized endfire arrays. The endfire antennas in [16], [18], and this work have asymmetric structures. The beam tilting in the vertical plane is observed in both [16] and [18] but is avoided in this work by using a modified transition plate. In [17], the two polarization antennas are placed parallel in order to lower the profile and achieve symmetric structure in the elevation plane. Therefore, the distance of the array elements is larger ($0.77\lambda_0$), which will lower the beam scanning angle. Comparing of all the other works, the proposed antenna has the smallest thickness due to the matching transitions plates, which, as a result, limits the bandwidth of the V-pol mode. In [11] and [12] the clearance of the broadside antennas is chosen as the ground plane width and in the other endfire antennas the clearance is applying the same rules as this work. The clearance in this work is larger than [16] but is much smaller than all the others.

IV. CONCLUSION

This paper proposes a dual-polarized endfire antenna at 28 GHz for 5G handset applications. It has planar structure with low profile of 1.1 mm and only 2.7 mm clearance. By utilizing the asymmetric transition plates to the SIW, the radiation patterns of the two

polarization are symmetric in the vertical plane over the operating band from 28 GHz to 30 GHz. The simulated cross-polarization is 10 dB lower than the co-polarization for both modes during the operating band. A 4-element array is implemented with the proposed dual-polarized antenna as array elements. The measured results of the array show good agreements with the simulations. The measured overlapping -10-dB bandwidth is from 27.5 GHz to 29 GHz and the cross-polarization is 10 dB lower than the co-polarization.

REFERENCES

- [1] W. Hong, K. Baek, and S. Ko, "Millimeter-wave 5g antennas for smartphones: Overview and experimental demonstration," *IEEE Transactions on Antennas and Propagation*, vol. 65, no. 12, pp. 6250–6261, Dec 2017.
- [2] J. G. Andrews, S. Buzzi, W. Choi, S. V. Hanly, A. Lozano, A. C. K. Soong, and J. C. Zhang, "What will 5g be?" *IEEE Journal on Selected Areas in Communications*, vol. 32, no. 6, pp. 1065–1082, June 2014.
- [3] Z. Tang, J. Liu, Y. Cai, J. Wang, and Y. Yin, "A wideband differentially fed dual-polarized stacked patch antenna with tuned slot excitations," *IEEE Transactions on Antennas and Propagation*, vol. 66, no. 4, pp. 2055–2060, April 2018.
- [4] K. M. Mak, H. W. Lai, and K. M. Luk, "A 5g wideband patch antenna with antisymmetric l-shaped probe feeds," *IEEE Transactions on Antennas and Propagation*, vol. 66, no. 2, pp. 957–961, Feb 2018.
- [5] Y. Cui, X. Gao, and R. Li, "A broadband differentially fed dual-polarized planar antenna," *IEEE Transactions on Antennas and Propagation*, vol. 65, no. 6, pp. 3231–3234, June 2017.
- [6] Z. Zhang and K. Wu, "A wideband dual-polarized dielectric magneto-electric dipole antenna," *IEEE Transactions on Antennas and Propagation*, vol. 66, no. 10, pp. 5590–5595, Oct 2018.
- [7] C. Wang, Y. Chen, and S. Yang, "Dual-band dual-polarized antenna array with flat-top and sharp cutoff radiation patterns for 2G/3G/LTE cellular bands," *IEEE Transactions on Antennas and Propagation*, vol. 66, no. 11, pp. 5907–5917, Nov 2018.
- [8] L. Wen, S. Gao, Q. Luo, C. Mao, W. Hu, Y. Yin, Y. Zhou, and Q. Wang, "Compact dual-polarized shared-dipole antennas for base station applications," *IEEE Transactions on Antennas and Propagation*, vol. 66, no. 12, pp. 6826–6834, Dec 2018.
- [9] Y. Cui, L. Wu, and R. Li, "Bandwidth enhancement of a broadband dual-polarized antenna for 2G/3G/4G and IMT base stations," *IEEE Transactions on Antennas and Propagation*, vol. 66, no. 12, pp. 7368–7373, Dec 2018.
- [10] Y. He, Z. Pan, X. Cheng, Y. He, J. Qiao, and M. M. Tentzeris, "A novel dual-band, dual-polarized, miniaturized and low-profile base station antenna," *IEEE Transactions on Antennas and Propagation*, vol. 63, no. 12, pp. 5399–5408, Dec 2015.
- [11] S. Liao and Q. Xue, "Dual polarized planar aperture antenna on ltcc for 60-ghz antenna-in-package applications," *IEEE Transactions on Antennas and Propagation*, vol. 65, no. 1, pp. 63–70, Jan 2017.
- [12] Y. Li and K. Luk, "60-GHz dual-polarized two-dimensional switch-beam wideband antenna array of magneto-electric dipoles," in *2015 IEEE International Symposium on Antennas and Propagation USNC/URSI National Radio Science Meeting*, July 2015, pp. 1542–1543.
- [13] "User Equipment (UE) Radio Transmission and Reception; Part 2: Range 2 Standalone (Release 15), document TS38.101-2 v15.4.0," Tech. Rep., 01 2019.
- [14] J. Helander, K. Zhao, Z. Ying, and D. Sjoberg, "Performance analysis of millimeter-wave phased array antennas in cellular handsets," *IEEE Antennas and Wireless Propagation Letters*, vol. 15, pp. 504–507, 2016.
- [15] K. Zhao, S. Zhang, Z. Ho, O. Zander, T. Bolin, Z. Ying, and G. F. Pedersen, "Spherical coverage characterization of 5g millimeter wave user equipment with 3gpp specifications," *IEEE Access*, vol. 7, pp. 4442–4452, 2019.
- [16] O. Jo, J. Kim, J. Yoon, D. Choi, and W. Hong, "Exploitation of dual-polarization diversity for 5g millimeter-wave mimo beamforming systems," *IEEE Transactions on Antennas and Propagation*, vol. 65, no. 12, pp. 6646–6655, Dec 2017.
- [17] A. Li, K. Luk, and Y. Li, "A dual linearly polarized end-fire antenna array for the 5g applications," *IEEE Access*, vol. 6, pp. 78 276–78 285, 2018.
- [18] Y. Hsu, T. Huang, H. Lin, and Y. Lin, "Dual-polarized quasi yagiuda antennas with endfire radiation for millimeter-wave mimo terminals," *IEEE Transactions on Antennas and Propagation*, vol. 65, no. 12, pp. 6282–6289, Dec 2017.
- [19] H. Jin, Y. M. Huang, H. Jin, and K. Wu, "e-band substrate integrated waveguide orthomode transducer integrated with dual-polarized horn antenna," *IEEE Transactions on Antennas and Propagation*, vol. 66, no. 5, pp. 2291–2298, May 2018.
- [20] M. Esquiús-Morote, B. Fuchs, J. Zrcher, and J. R. Mosig, "A printed transition for matching improvement of siw horn antennas," *IEEE Transactions on Antennas and Propagation*, vol. 61, no. 4, pp. 1923–1930, April 2013.
- [21] L. Wang, M. Esquiús-Morote, H. Qi, X. Yin, and J. R. Mosig, "Phase corrected H -plane horn antenna in gap siw technology," *IEEE Transactions on Antennas and Propagation*, vol. 65, no. 1, pp. 347–353, Jan 2017.
- [22] "General aspects for user equipment (ue) radio frequency (rf) for nr, technical report (tr) tr38.817-01," Tech. Rep., 01 2019.
- [23] F. Ren, W. Hong, and K. Wu, "Three-dimensional siw-driven microstrip antenna for wideband linear and circular polarization applications," *IEEE Antennas and Wireless Propagation Letters*, vol. 16, pp. 2400–2403, 2017.
- [24] W. El-Halwagy, R. Mirzavand, J. Melzer, M. Hossain, and P. Mousavi, "Investigation of wideband substrate-integrated vertically-polarized electric dipole antenna and arrays for mm-wave 5g mobile devices," *IEEE Access*, vol. 6, pp. 2145–2157, 2018.